Tissue Reflectivity Function Restoration from Fundamental and Harmonic Ultrasound Images

Mohamad Hourani
University of Toulouse
IRIT/INP-ENSEEIHT
IRIT, CNRS UMR 5505
Toulouse, France

Adrian Basarab
University of Toulouse
Université Paul Sabatier
IRIT, CNRS UMR 5505
Toulouse, France

Denis Kouamé
University of Toulouse
Université Paul Sabatier
IRIT, CNRS UMR 5505
Toulouse, France

Jean-Yves Tourneret
University of Toulouse
IRIT/INP-ENSEEIHT
IRIT, CNRS UMR 5505
Toulouse, France

***Abstract*—This paper addresses the problem of ultrasound (US) image restoration. In contrast to most of the existing approaches that only take into account fundamental radiofrequency (RF) data, the proposed method also considers harmonic US images. An algorithm based on the alternating direction of multipliers method (ADMM) is proposed to solve the joint deconvolution problem. Simulation results show the interest of the proposed approach when compared to classical US image restoration schemes based only on fundamental data.**

I. Image model

Ultrasound (US) image formation is based on the propagation of US waves inside human tissues. These waves are produced by piezoelectric elements of the US probe, and correspond to short pulses at a given central frequency. While propagating, wave distortions may occur creating backscattered echoes at multiples of the US probe central frequency and forming the so-called tissue harmonic images. However, because of the strong attenuation, only the first harmonic is exploited in most applications. Tissue harmonic imaging presents several advantages compared to conventional (fundamental) US imaging, such as better spatial resolution and improved contrast to noise ratio [1]. However, harmonic images have also an important drawback related to high attenuation with imaging depth. Building a mathematical model relating the unknown US image, referred to as tissue reflectivity function (TRF), to the observed fundamental and harmonic images has been the object of recent research studies. Although a nonlinear equation characterizes the propagation of US waves in biological tissues, a linear model is classically used, motivated by weak scattering conditions in US [2], [3]. Specifically, US images are modeled as the convolution between the imaging system PSF and the TRF. In this study, two linear models are used for the fundamental and harmonic images. These models are defined as follows:

$$\boldsymbol{y_f} = H_f \boldsymbol{r} + \boldsymbol{n_f} \quad (1)$$

$$\boldsymbol{y_h} = W H_h \boldsymbol{r} + \boldsymbol{n_h}, \quad (2)$$

where $y_f \in \mathbb{R}^N$ and $y_h \in \mathbb{R}^N$ are the observed fundamental and harmonic radiofrequency RF images that have been vectorized in lexicographical order, $\boldsymbol{r} \in \mathbb{R}^N$ is the unknown TRF to be estimated, H_f and $H_h \in \mathbb{R}^{N\times N}$ are block circulant with circulant blocks matrices accounting for 2D convolution with circulant boundary conditions, $\boldsymbol{n_f}$ and $\boldsymbol{n_h} \in \mathbb{R}^N$ are additive white Gaussian noises and $W \in \mathbb{R}^{N\times N}$ is a diagonal matrix gathering the attenuation coefficients for each image depth. Estimating $\boldsymbol{r}$ from y_f and y_h is formulated in this work as the following minimization problem:

$$\min_{\boldsymbol{r}} \frac{1}{2}\|\boldsymbol{y_f} - H_f \boldsymbol{r}\|_2^2 + \frac{1}{2}\|\boldsymbol{y_h} - W H_h \boldsymbol{r}\|_2^2 + \mu\|\boldsymbol{r}\|_1 \quad (3)$$

where $||.||_1$ is the ℓ_1-norm that is commonly used for regularizing the TRF solution, see, e.g., [4], [5].

II. TRF restoration algorithm

In order to solve (3), we propose to use the well-known ADMM framework [6] classically used to solve problems of the form

$$\min_{u,v} \quad f_1(\boldsymbol{u}) + f_2(\boldsymbol{v}) \ \text{ s.t. } A\boldsymbol{u} + B\boldsymbol{v} = c \quad (4)$$

where f_1 and f_2 are closed convex functions and A, B and $\boldsymbol{u}, \boldsymbol{v}, \boldsymbol{c}$ are matrices and vectors of appropriate sizes. We reformulate (3) as

$$\min_{\boldsymbol{u}} \frac{1}{2}\|\boldsymbol{y_f} - H_f \boldsymbol{u}\|_2^2 + \frac{1}{2}\|\boldsymbol{y_h} - W\boldsymbol{z}\|_2^2 + \mu\|\boldsymbol{w}\|_1 \quad (5)$$

where $\boldsymbol{z} = H_h \boldsymbol{r}$, $\boldsymbol{w} = \boldsymbol{u} = \boldsymbol{r}$, and we introduce the vector $\boldsymbol{v} = \left[\begin{smallmatrix}\boldsymbol{w}\\ \boldsymbol{z}\end{smallmatrix}\right]$. The minimization problem (5) fits the general framework of ADMM in (4) by choosing $f_1(u) = \frac{1}{2}\|\boldsymbol{y_f} - H_f\boldsymbol{u}\|_2^2$, $f_2(v) = \frac{1}{2}\|\boldsymbol{y_h} - W\boldsymbol{z}\|_2^2 + \mu\|\boldsymbol{w}\|_1$, $A = \left[\begin{smallmatrix} I_N \\ H_h \end{smallmatrix}\right]$, $B = \left[\begin{smallmatrix} -I_N & 0 \\ 0 & -I_N \end{smallmatrix}\right]$ and $c = 0_N$. As a consequence, (5) can be solved by an iterative algorithm (iterations are denoted by k) minimizing the associated augmented Lagrangian $\mathcal{L}_A(\boldsymbol{u}, \boldsymbol{v}, \boldsymbol{\lambda})$ with respect to each variable, with the Lagrangian multiplier $\boldsymbol{\lambda} = [\boldsymbol{\lambda}_1\ \boldsymbol{\lambda}_2]^T$. The resulting variable updates are summarized below (see Algo.1 for further details)

Step 1: Update $\boldsymbol{u}$ using an analytical solution in the Fourier domain (see Algo.1, lines 3 and 4):

$$\boldsymbol{u^{k+1}} \in \operatorname{argmin}_{\boldsymbol{u}} \frac{1}{2}\|\boldsymbol{y_f} - H_f\boldsymbol{u}\|_2^2 + \frac{\beta}{2}\|A\boldsymbol{u} + B\boldsymbol{v^k} + \frac{\boldsymbol{\lambda^k}}{\beta}\|_2^2 \quad (6)$$

Step 2.1: Update $\boldsymbol{w}$ using the soft thresholding operator associated with the ℓ_1-norm [7] (see Algo.1, line 6):

$$\boldsymbol{w^{k+1}} \in \operatorname{argmin}_{\boldsymbol{w}} \ \mu\|\boldsymbol{w}\|_1 + \frac{\beta}{2}\|\boldsymbol{u^{k+1}} - \boldsymbol{w} + \frac{\boldsymbol{\lambda_1^k}}{\beta}\|_2^2 \quad (7)$$

Step 2.2: Update $\boldsymbol{z}$ using an analytical solution (Algo. 1, line 7).

$$\boldsymbol{z^{k+1}} \in \operatorname{argmin}_{\boldsymbol{w}} \ \frac{1}{2}\|\boldsymbol{y_h} - W\boldsymbol{z}\|_2^2 + \frac{\beta}{2}\|H_h\boldsymbol{u^{k+1}} - \boldsymbol{z} + \frac{\boldsymbol{\lambda_2^k}}{\beta}\|_2^2 \quad (8)$$

Step 3: Update the Lagrangian multiplier $\boldsymbol{\lambda}$ (see Algo. 1, line 8).

III. Experiments and results

The performance of the proposed algorithm is evaluated on a simulated image with controlled ground truth. The results are compared to a classical TRF restoration scheme based only on the fundamental data, *i.e.*, that solves (3) without the second data fidelity term. To generate the fundamental and harmonic images, the TRF mimicking a human kidney was convolved with two PSFs of central frequency 3.5 MHz and 7 MHz. Furthermore, the harmonic image was attenuated with depth, as highlighted in Fig. 1(d). The resulting images and quantitative results are reported in Fig. 1 and in Tab. I. They show the gain in estimation performance due to the joint use of fundamental and harmonic images.

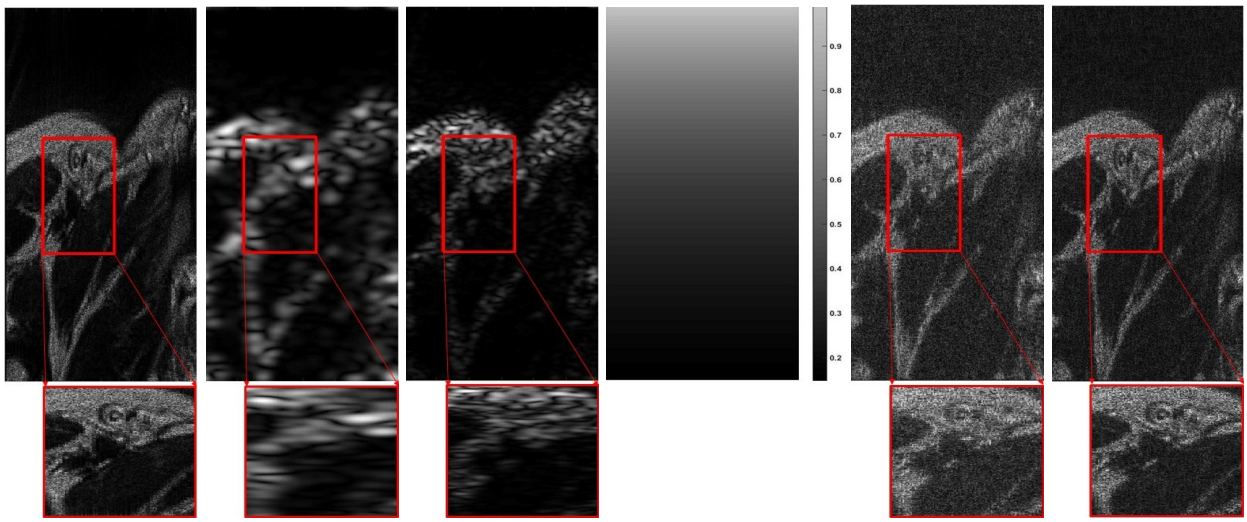

(a) (b) (c) (d) (e) (f)

Fig. 1: (a) TRF mimicking a human kidney ($\boldsymbol{r}$ of size 1300×300 pixels), (b) simulated fundamental image $\boldsymbol{y_f}$, (c) simulated harmonic image $\boldsymbol{y_h}$, (d) attenuation map used to simulate the harmonic image in (c), with value equal to 1 (no attenuation) close to the probe and 0.1 (high attenuation) at the bottom of the image, (e) TRF estimated by LASSO from the fundamental US image in (b), (f) TRF estimated by the proposed method from fundamental and harmonic US images in (b) et (c). Note that all US images are shown, for visualization purpose, in B-mode (log-compressed demodulated RF images). A zoom of the region in the red rectangle allows to appreciate fine details in the ground truth TRF, observed images and restored TRFs.

Algorithm 1: Proposed TRF algorithm in US imaging

Input: $\boldsymbol{y_f}$, $\boldsymbol{y_h}$, H_f, H_h

Set $k = 0$, $\mu > 0$, $\beta > 0$, $\boldsymbol{u^0}$, $\boldsymbol{v^0}$, $\boldsymbol{\lambda^0}$, k_{max}, i_{max}, tol

while *no convergence* ***and*** $k < k_{max}$ **do**

// Step 1: Analytical solution of (6)

$$\boldsymbol{u}^{k+1} \leftarrow (H_f^T H_f + \beta H_h^T H_h + \beta I_N)^{-1}(H_f^T y_f + \beta H_h^T \boldsymbol{z}^k - \boldsymbol{\lambda_1^k} - H_h^T \boldsymbol{\lambda_2^k} + \beta \boldsymbol{w}^k);$$

// Solution of (6) *in the Fourier Domain* [1]

$$\boldsymbol{u}^{k+1} \leftarrow F^*(\Lambda_f^* \Lambda_f + \beta \Lambda_h^* \Lambda_h + \beta I_N)^{-1}(\Lambda_f^* F y_f + \beta \Lambda_f^* F \boldsymbol{z}^k - F\boldsymbol{\lambda_1^k} - \Lambda_f^* F \boldsymbol{\lambda_2^k} + \beta F \boldsymbol{w}^k);$$

// Step 2.1: Solution of (7) *by soft thresholding*

$$t^k = \boldsymbol{u}^{k+1} + \boldsymbol{\lambda_1^k}/\beta;$$

$$\boldsymbol{w}^{k+1} \leftarrow soft_{\frac{\mu}{\beta}}(t^k) = max(|t^k| - \frac{\mu}{\beta}, 0) sign(t^k);$$

// Step 2.2: Analytical solution of (8)

$$\boldsymbol{z^{k+1}} \leftarrow (W^T W + \beta I_N)^{-1}(W^T y_h + \beta H_h u^{k+1} + \lambda_2^k);$$

// Step 3: Update Lagrangian multiplier

$$\boldsymbol{\lambda}^{k+1} = \boldsymbol{\lambda}^k + \beta(A\boldsymbol{u}^{k+1} + B\boldsymbol{v}^{k+1});$$

$k \leftarrow k + 1$;

end

// [1] *where:*

- H_f *and* H_f *BCCB matrix* $\Rightarrow H_f = F^* \Lambda_f F$ *and* $H_h = F^* \Lambda_h F$.
- F *and* F^* *are the Fourier and inverse Fourier transforms.*
- $\Lambda_f = diag(F\boldsymbol{l}_f)$ *and* $\Lambda_h = diag(F\boldsymbol{l}_h)$.
- $\boldsymbol{l}_f$ *and* $\boldsymbol{l}_h$ *stands for the first column of the blurring matrix* H_f *and* H_h.

	SSIM$(\%)$	**RMSE**	**ISNR**(dB)
Lasso	29.59	0.0929	4.637
Proposed method	**61.18**	**0.0602**	**6.757**

TABLE I: Quantitative results corresponding to the selected regions (in red) of images in Fig. 1, computed using the estimated and ground truth TRF. SSIM stands for structure similarity index [8], RMSE is the root mean squared error and ISNR the improvement in signal-to-noise ratio.

REFERENCES

[1] F. Tranquart, N. Grenier, V. Eder, and L. Pourcelot, "Clinical use of ultrasound tissue harmonic imaging," *Ultrasound in Medicine and Biology*, vol. 25, no. 6, pp. 889–894, 1999.

[2] J. Ng, R. Prager, N. Kingsbury, G. Treece, and A. Gee, "Modeling ultrasound imaging as a linear, shift-variant system," *IEEE Trans. Ultrason., Ferroelectr., Freq. Control*, vol. 53, no. 3, pp. 549–563, 2006.

[3] R. J. Zemp, C. K. Abbey, and M. F. Insana, "Linear system models for ultrasonic imaging: Application to signal statistics," *IEEE Trans. Ultrason., Ferroelectr., Freq. Control*, vol. 50, no. 6, pp. 642–654, 2003.

[4] Z. Chen, A. Basarab, and D. Kouamé, "Compressive deconvolution in medical ultrasound imaging," *IEEE Trans. Med. Imag.*, vol. 35, no. 3, pp. 728–737, 2016.

[5] O. V. Michailovich and D. Adam, "A novel approach to the 2-d blind deconvolution problem in medical ultrasound," *IEEE Trans. Med. Imag.*, vol. 24, no. 1, pp. 86–104, 2005.

[6] S. Boyd, N. Parikh, E. Chu, B. Peleato, and J. Eckstein, "Distributed optimization and statistical learning via the alternating direction method of multipliers," *Foundations and Trends in Machine Learning*, vol. 3, no. 1, pp. 1–122, 2011.

[7] Z. Chen, A. Basarab, and D. Kouamé, "Reconstruction of enhanced ultrasound images from compressed measurements using simultaneous direction method of multipliers," *IEEE Trans. Ultrason., Ferroelectr., Freq. Control*, vol. 63, no. 10, pp. 1525–1534, Oct 2016.

[8] Z. Wang, A. C. Bovik, H. R. Sheikh, and E. P. Simoncelli, "Image quality assessment: from error visibility to structural similarity," *IEEE Trans. Image Process.*, vol. 13, no. 4, pp. 600–612, 2004.